



La Science à l'œuvre pour le  
at work for Canada

## NRC Publications Archive Archives des publications du CNRC

### **A numerical investigation on soot formation from laminar diffusion flames of ethylene/methane mixture.**

Guo, Hongsheng; Trottier, Stephanie; Johnson, Matthew R.; Smallwood, Gregory

### **NRC Publications Record / Notice d'Archives des publications de CNRC:**

<http://nparc.cisti-icist.nrc-cnrc.gc.ca/npsi/ctrl?action=rtdoc&an=6421208&lang=en>

<http://nparc.cisti-icist.nrc-cnrc.gc.ca/npsi/ctrl?action=rtdoc&an=6421208&lang=fr>

Access and use of this website and the material on it are subject to the Terms and Conditions set forth at

[http://nparc.cisti-icist.nrc-cnrc.gc.ca/npsi/jsp/nparc\\_cp.jsp?lang=en](http://nparc.cisti-icist.nrc-cnrc.gc.ca/npsi/jsp/nparc_cp.jsp?lang=en)

READ THESE TERMS AND CONDITIONS CAREFULLY BEFORE USING THIS WEBSITE.

L'accès à ce site Web et l'utilisation de son contenu sont assujettis aux conditions présentées dans le site

[http://nparc.cisti-icist.nrc-cnrc.gc.ca/npsi/jsp/nparc\\_cp.jsp?lang=fr](http://nparc.cisti-icist.nrc-cnrc.gc.ca/npsi/jsp/nparc_cp.jsp?lang=fr)

LISEZ CES CONDITIONS ATTENTIVEMENT AVANT D'UTILISER CE SITE WEB.

Contact us / Contactez nous: [nparc.cisti@nrc-cnrc.gc.ca](mailto:nparc.cisti@nrc-cnrc.gc.ca).



National Research  
Council Canada

Conseil national  
de recherches Canada

Canada

## ASME HT2008-56151

# A Numerical Investigation on Soot Formation from Laminar Diffusion Flames of Ethylene/Methane Mixture

Hongsheng Guo<sup>1</sup>, Stephanie Trottier<sup>2</sup>, Matthew R. Johnson<sup>3</sup>, Gregory J. Smallwood<sup>1</sup>

<sup>1</sup>Institute for Chemical Process and Environmental Technology, National Research Council Canada, 1200 Montreal Road, Ottawa, Ontario, Canada K1A 0R6

<sup>2</sup>Albert Research Council Inc., 250 Karl Clark Road, Edmonton, Alberta, Canada T6N 1E4

<sup>3</sup>Dept. of Mechanical & Aerospace Engineering, Carleton University, Ottawa, Ontario, Canada K1S 5B6

### ABSTRACT

The sooting propensity of laminar diffusion flames employing ethylene/methane mixture fuel is investigated by numerical simulation. Detailed gas phase chemistry and moments method are used to describe the chemical reaction process and soot particle dynamics, respectively. The numerical model captures the primary features experimentally observed previously. At constant temperatures of air and fuel mixture, both maximum soot volume fraction and soot yield monotonically decrease with increasing the fraction of carbon from methane in the fuel mixture. However, when the temperatures of air and fuel mixture are preheated so that the adiabatic temperatures of all flames are same, the variation of the maximum soot yield becomes higher than what would be expected from a linear combination of the flames of pure ethylene and pure methane, showing a synergistic phenomenon in soot formation. Further analysis of the details of the numerical results suggests that the synergistic phenomenon is caused by the combined effects of the variations in the concentrations of acetylene ( $C_2H_2$ ) and methyl radical ( $CH_3$ ). When the fraction of carbon from methane in fuel mixture increases, the concentration of  $C_2H_2$  monotonically decreases, whereas that of methyl radical increases, resulting in a synergistic phenomenon in the variation of propargyl ( $C_3H_3$ ) radical concentration due to the reactions  $C_2H_2 + CH_3 = PC_3H_4 + H$  and  $PC_3H_4 + H = C_3H_3 + H_2$ . This synergistic phenomenon causes a qualitatively similar variation trend in the concentration of pyrene (A4) owing to the reaction paths  $C_3H_3 \rightarrow A1$  (benzene)  $\rightarrow A2$  (naphthalene)  $\rightarrow A3$  (phenanthrene)  $\rightarrow$

A4. Consequently, the synergistic effect occurs for soot inception and PAH condensation rates, leading to the synergistic phenomenon in soot yield. The similar synergistic phenomenon is not observed in the variation of peak soot volume fraction, since the maximum surface growth rate monotonically decreases, as the fraction of carbon from methane in fuel mixture increases.

### INTRODUCTION

Soot is one of primary pollutants emitted during the combustion of fossil fuels. Emission of soot not only has a detrimental effect on human health, but also contributes significantly to global warming. Therefore, various restrictions are being placed on soot emission today. Strategies are needed to control and reduce soot emission. Quantitative understanding of soot formation mechanism is crucial to the development of strategies for reducing soot emission.

Soot formation in elemental fuel combustion has been extensively investigated. Relatively, the study on soot formation in the combustion of binary fuels or fuel mixtures is limited. In the literature, there is conflicting experimental evidence of the existence of synergistic phenomenon in soot formation of binary fuels [1,2]. In this context, a synergistic phenomenon means that soot formation in the flame of a mixture fuel is higher than the linear combination of the flames of both pure fuels. Frenklach [1] showed the presence of such a synergistic phenomenon in soot formation of numerous mixtures and indicated that the phenomenon could be due to the acetylene based inception and growth mechanisms. Hwang et

al. [2,3] investigated the effects of propane and oxygen addition on soot formation in ethylene diffusion flames. They observed a synergistic phenomenon in soot formation with the addition of propane or oxygen to ethylene, and attributed the enhancement in soot formation with propane and oxygen addition to the propargyl ( $C_3H_3$ ) re-combination reaction. This conclusion challenged the early PAH and soot formation reaction scheme [4] that suggested that the first aromatic ring was formed by the addition of acetylene to C4 radicals and the key growth process toward large PAH occurred by continuous addition of acetylene ( $C_2H_2$ ), but was qualitatively consistent with the assumption that benzene could be formed, in large part, from the re-combination of resonantly-stabilized propargyl radicals [5]. Roesler et al. [6] investigated the role of methane on the growth of aromatic hydrocarbons and soot, and also found that the existence of a synergistic chemical effect between methane and other alkanes in the production of aromatics, despite reduced acetylene concentrations. They concluded that the synergistic phenomenon was caused by the ability of methane to produce methyl ( $CH_3$ ) radical that promoted production channels of aromatics that relied on odd-carbon-numbered species, such as propargyl ( $C_3H_3$ ). More recently, Trottier et al. [7] carried out a detailed study on the sooting propensity of various binary fuel mixtures, and observed the synergistic phenomenon in some mixtures but not in others. Further analysis of [7] also suggested that the synergistic phenomenon resulted from the enhanced production of  $CH_3$  radical. McEnally and Pfefferle [8] measured soot volume fractions along the centerline of ethylene/air nonpremixed flames when dimethyl ether (DME) and ethanol (EtOH) were added, and found that the addition of either DME or EtOH enhanced the soot volume fraction, although pure DME and EtOH diffusion flames produced less soot than ethylene. Their measured profiles of C1-C12 hydrocarbons implied that due to the increased  $CH_3$ , the addition of DME and EtOH enhanced the rate of C1 + C2 addition reactions that formed propargyl radical and consequently enhanced the formation of benzene through propargyl re-combination, resulting in the increase in soot formation. Apparently, most of these studies attributed the synergistic phenomenon of soot formation in binary fuel mixtures to the increased  $CH_3$  radical through its role in the formation of propargyl and finally benzene.

A complete understanding of the synergistic phenomenon needs both experimental and numerical studies. Details of numerical results for the combustion of binary fuel mixtures can help not only identify the mechanism of the synergistic phenomenon, but also validate the chemistry and soot model. Most above studies on the synergistic phenomenon were by experiments. Two of them contained numerical investigations, but they either completely neglected soot [3] or employed simplified soot model [7]. Therefore, it is necessary to further investigate the synergistic phenomenon in the combustion of binary fuel mixtures by detailed numerical simulation.

In this paper, a detailed numerical study on the synergistic phenomenon in soot formation from the diffusion flames of ethylene/methane mixtures is carried out. The purpose is to further identify the mechanism of the synergistic effects by the details from numerical simulation, and validate the existing chemical reaction scheme and soot model. We focus on the ethylene/methane mixtures, since pure ethylene/air diffusion

flames have been extensively studied both experimentally and numerically, and the addition of methane can promote the formation of  $CH_3$  radical. The numerical model is described first. Then the results of simulation are compared with the experimental data of [7] for soot volume fraction and the maximum soot yield, followed by discussion using the details of numerical results.

## NUMERICAL MODEL

The flames modeled in this paper are those employing ethylene/methane mixture fuel in our previous experimental study [7]. They were generated at atmospheric pressure with a burner in which the ethylene/methane fuel mixture issued from a 10.9 mm inner diameter vertical tube, and the oxidant (air) from the annular region between the fuel tube and a 100 mm diameter concentric tube. Soot volume fraction was measured by line-of-sight-attenuation (LOSA) optical diagnostic method. More details of the experiments can be found from [7].

To have a proper basis for comparison and be consistent with experiments, the carbon content of the fuel mixture is kept constant at a fixed carbon flow rate of 3.2 mg/s in all flames, while the contribution of each component (ethylene or methane) to the total carbon in the mixture varies from 0 to 100%. The flow rate of the co-flow air is 284 L/min at room temperature and atmospheric pressure condition.

Two sets of flames are studied. Both fuel mixture and air are at room temperature in the first set of flames (non-preheated case), whereas the fuel mixture and air are preheated so that the adiabatic temperatures of all flames are the same as that of the pure ethylene flame in the second set (preheated case).

The formation and evolution of soot particles are modeled by the method of moments [9]. The soot particle moments are defined as

$$M_r = \sum_{i=1}^{\infty} m_i^r N_i \quad (1)$$

where  $M_r$  is the  $r$ th moment of soot particle distribution, and  $m_i$  and  $N_i$  are the mass and the particle number density, respectively, of the soot particles of size class  $i$ . The soot particle mass is represented by the number of carbon atoms. In this paper, six concentration moments (i.e.  $M_r = M_1, M_2, M_3, M_4, M_5, M_6$ ) are used.

The governing equation for each soot concentration moment is

$$\begin{aligned} \rho u \frac{\partial (M_r / \rho)}{\partial z} + \rho v \frac{\partial (M_r / \rho)}{\partial r} = & \\ \frac{\partial}{\partial z} \left( \rho D_{p,1} \frac{\partial}{\partial z} \left( \frac{M_{r-2/3}}{\rho} \right) \right) + & \\ \frac{1}{r} \frac{\partial}{\partial r} \left( r \rho D_{p,1} \frac{\partial}{\partial r} \left( \frac{M_{r-2/3}}{\rho} \right) \right) & \\ - \frac{\partial}{\partial z} (V_{T,z} M_r) - \frac{1}{r} \frac{\partial}{\partial r} (r V_{T,r} M_r) + Q_r & \end{aligned} \quad (2)$$

where  $\rho$  is density ( $g/cm^3$ ),  $u$  and  $v$  the axial ( $z$ ) and radial ( $r$ ) direction velocities (cm/s), respectively,  $Q_r$  the source term, and

$M_{r-2/3}$  the fractional moments obtained by interpolation between the whole moments. Quantity  $V_{T,x_i}$  is the thermal diffusion velocity of soot in  $z$  or  $r$  direction, and is calculated by [11]

$$V_{T,x_i} = -0.55 \frac{\nu}{T} \frac{\partial T}{\partial x_i} \quad (x_i = z \text{ or } r) \quad (3)$$

where  $\nu$  is the kinematic viscosity. Quantity  $D_{p,i}$  is the diffusion rate of the smallest soot particles, and is given by [9]

$$D_{p,i} = \frac{3}{2\rho} \sqrt{\frac{\overline{m} k_B T}{2\pi}} \left(1 + \frac{\pi\alpha_T}{8}\right)^{-1} \frac{1}{d_i^2} \quad (4)$$

with  $\overline{m}$  being the mean mass of the gas (g),  $K_B$  the Boltzmann's constant (erg mol<sup>-1</sup> K<sup>-1</sup>),  $T$  the temperature (K),  $\alpha_T$  the thermal accommodation coefficient (0.9), and  $d_i$  the diameter of the smallest soot particle (cm). The source term  $Q_r$  in each moment equation accounts for particle nucleation, coagulation, surface growth and oxidation of soot particles.

The nucleation is assumed to be due to the coalescence of two large size PAH, pyrene (A4), into a dimer. Then the particle size increases or decreases due to the particle coagulation, surface growth and oxidation.

The gas phase reaction scheme and the calculation methods for the particle nucleation, coagulation, surface growth and oxidation are basically those developed by Appel et al. [10]. Although the methods and gas phase chemistry of Appel et al. have been validated by several premixed flames, soot volume fraction was significantly underpredicted when they were directly used for the diffusion flames of this paper. Therefore, several modifications are made.

The first modification is to limit the particle coagulation by setting the coagulation rate as zero when the mean particle diameter is greater than 25 nm. This is based on the experimental observation that generally the maximum diameter of a primary particle is about 25 ~ 30 nm.

Then we increase the surface growth rate by changing the acetylene (C<sub>2</sub>H<sub>2</sub>) addition rate and the parameter  $\alpha$  – the fraction of surface sites available for surface reactions. The reaction rate of acetylene addition provided by Appel et al. [10] is increased by five times in this paper. The parameter  $\alpha$  is still calculated by the Eq. 1 of Appel et al. [10], but the parameter  $a$  in the equation is increased by 3 times, and the parameter  $b$  is modified to  $b = -1.38 + 1.02 \times 10^{-3} \times T$ , with  $T$  being local temperature.

After above modifications, the peak soot volume fractions were reasonably predicted. However, soot volume fractions in the centerline region were still significantly underpredicted. Realizing that the chemistry developed by Appel et al. [10] underpredicted the concentration of pyrene (the inception PAH species) in some flames, we reduce the scrubbing factor of pyrene  $\alpha_{A4}$  to 0.003, i.e. the reaction rate of pyrene is calculated by  $r_{A4} = r_{g,A4} + \alpha_{A4} \cdot r_{s,A4}$ , where  $r_{A4}$ ,  $r_{g,A4}$ ,  $r_{s,A4}$  and  $\alpha_{A4}$  are, respectively, the net rate, the rate due to gas phase reactions, the rate due to soot formation and the scrubbing factor of pyrene. This treatment is an *ad hoc* one. The scrubbing factors of all other species are unity. Other details of the soot model are

the same as those given by Appel et al. [10]. The free molecular regime is employed for the calculation of coagulation.

The governing equations for conservation of mass, momentum, energy and gas species mass fractions can be found elsewhere [11]. Low Mach number assumption is adopted. The governing equations are discretized using the finite volume method in axisymmetric cylindrical coordinates. The SIMPLE numerical scheme [12] is used to handle the pressure and velocity coupling. The diffusion terms in the conservation equations are discretized by the central difference method and the convective terms are discretized by the power law method [12]. To speed up the convergent process, the governing equations of gas species and soot moments are, respectively, solved in a fully coupled fashion at each control volume [13]. Those of momentum, energy and pressure correction are solved using the tri-diagonal matrix algorithm.

The computational domain covers an area from 0 to 3.0 cm in the radial direction and 0 to 11.0 cm in the axial direction. The inflow boundary ( $z = 0$  cm) corresponds to the region immediately above the fuel nozzle. Totally 160 ( $z$ )  $\times$  105 ( $r$ ) non-uniform grids are used in the simulations, with finer grids placed in the primary reaction zone and near the fuel nozzle exit region. It has been checked that the further increase of grid number does not significantly influence the simulation results. The thermal and transport properties are obtained by using the algorithms given by [14,15].

Radiation heat transfer is calculated by the method given by Liu et al. [16]. Other details of the numerical methods can be found from our previous publication [11].

## RESULTS AND DISCUSSION

Unless explicitly indicated, all the experimental data below are taken from our previous study [7].

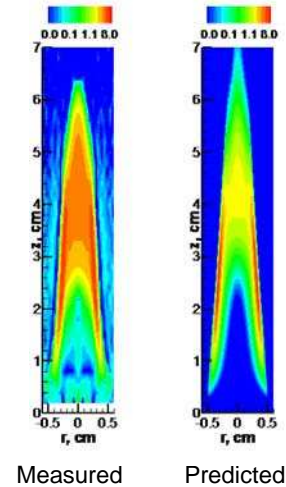


Fig. 1 Calculated and measured soot volume fraction (ppm) in pure ethylene/air flame.

Figure 1 shows the measured [7] and calculated soot volume fraction of pure ethylene flame. It is observed that although the simulation slightly underpredicts the soot volume fraction in the centreline region, it has basically captured the

primary features of soot in the flame. The peak soot volume fraction and the distributions of soot are reasonably predicted.

Figure 2 shows the variation of the maximum soot volume fraction when the fraction of carbon from methane in the fuel mixture changes from 0.0 (pure ethylene) to 1.0 (pure methane). We observe that when the fuel mixture is gradually changed from pure ethylene to pure methane, the maximum soot volume fraction monotonically decreases. The decrease slows down when both fuel mixture and air are preheated so that the adiabatic temperatures of all flames are the same as that of pure ethylene flame. However, there is not any synergistic behaviour. This is slightly different from the observation of Roesler et al. [6], who observed a synergistic behaviour for peak soot volume fraction. Although we are not sure what causes the difference, the different scenarios used in [6] and [7] might be one reason. The numerical simulation captures the basic feature of the maximum soot volume fraction, although there is a quantitative difference between simulation and experiment.

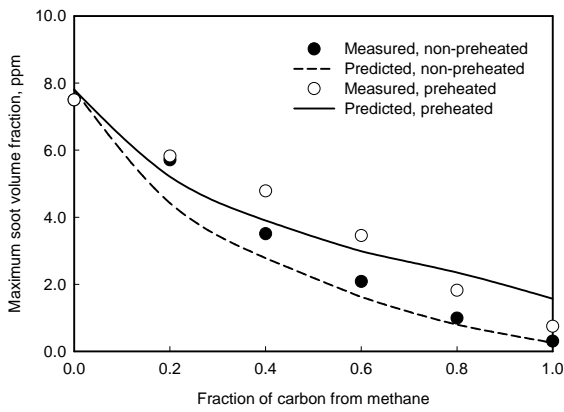


Fig. 2 Variation of the maximum soot volume fraction.

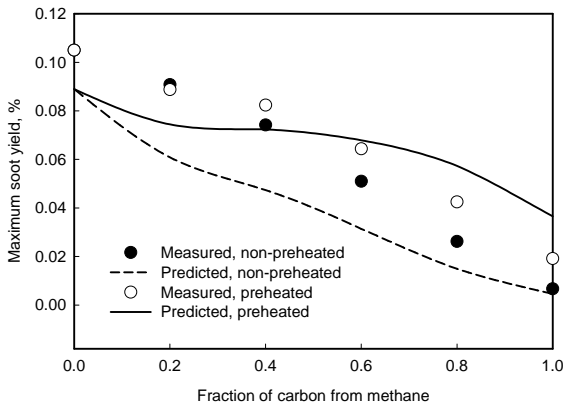


Fig. 3 Variation of the maximum soot yield.

Figure 3 shows the variation of the maximum soot yield with increasing the fraction of carbon from methane. The soot yield (%) is defined as

$$Y_s = \frac{\int 2\pi r u \rho_s f_v dr}{m_c} \cdot 100 \quad (5)$$

where  $u$  is the velocity (cm/s),  $\rho_s$  is the density of soot ( $1.9 \text{ g/m}^3$ ),  $f_v$  is soot volume fraction, and  $m_c$  is the mass flux of carbon from the fuel mixture ( $3.2 \text{ mg/s}$ ). We observe again that the simulation captures the primary features of experiment. For the non-preheated case, there is no any synergistic phenomenon. However, for the preheated case, the maximum soot yield becomes higher than what would be expected from a linear combination of pure ethylene and methane flames, showing the presence of a synergistic phenomenon. We shall discuss how the synergistic phenomenon occurs in the preheated case of ethylene/methane mixture below by using the details from numerical simulation. Unless explicitly indicated, all the data in Figs. 4-10 are from simulation.

Soot formation consists of inception, surface growth and oxidation processes. The oxidation occurs mainly in the upper flame region. In the lower flame region, where most soot is formed, inception and surface growth dominates. Therefore, we'll examine how inception and surface growth rates change over the range of ethylene/methane mixture.

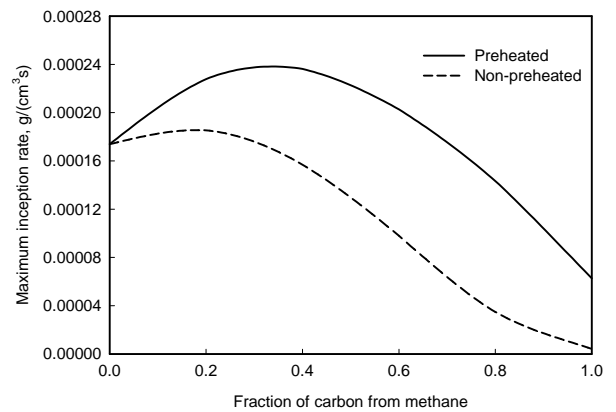


Fig. 4 Variation of the maximum inception rate.

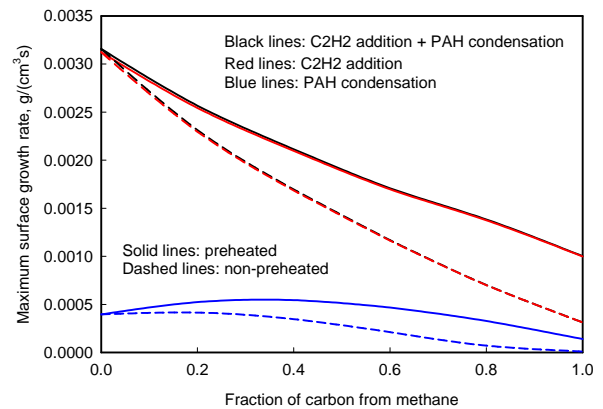


Fig. 5 Variations of the maximum surface growth,  $\text{C}_2\text{H}_2$  addition and PAH condensation rates.

Figure 4 shows the variation of the maximum inception rate for both preheated and non-preheated cases. It is illustrated that for the preheated case, the maximum inception rate first significantly increases and then decreases, showing a synergistic phenomenon, when the fraction of carbon from methane increases. Differently, for the non-preheated case, the

maximum inception rate only slightly increases and then quickly decreases. Although not shown, the simulation also suggests that the maximum inception rate in a flame usually occurs in the centreline region.

Figure 5 displays the variations of the maximum surface growth rate. Since surface growth consists of acetylene ( $C_2H_2$ ) addition and PAH condensation, the maximum rates of both these two sub-processes are shown. Firstly, by comparing Figs. 4 and 5, we observe that surface growth rate is more than one order of magnitude higher than inception rate for both preheated and non-preheated cases, meaning that surface growth dominates soot formation in terms of total soot mass formed. Secondly, Fig. 5 shows that the maximum total surface growth rate (black lines) is only slightly higher than the maximum  $C_2H_2$  addition rate (red lines) for all flames, indicating that  $C_2H_2$  addition dominates surface growth in the maximum surface growth rate region. These observations are consistent with the current understanding of soot formation in the literature.

For both preheated and non-preheated cases, no synergistic phenomenon can be observed for the maximum  $C_2H_2$  addition and total surface growth rates over the range of the ethylene/methane mixture fuel. The maximum  $C_2H_2$  addition and the total surface growth rates monotonically decrease with the increase in the fraction of carbon from methane in the fuel mixture. However, a strong synergistic phenomenon is observed for the maximum PAH condensation of the preheated case, and a slight one is observed for that of the non-preheated case. Please note that in Fig. 5, the summation of the maximum  $C_2H_2$  addition and PAH condensation rates does not equal the maximum total surface growth rate, because the positions of the maximum  $C_2H_2$  addition and PAH condensation are different. Usually the maximum  $C_2H_2$  addition and total surface growth occur in the flame wing region (near the maximum soot volume fraction region, as in Fig. 1). Alternately, being similar to inception, the maximum PAH condensation occurs in the centreline region of a flame.

Above results of inception and surface growth rates can explain the variations of the maximum soot volume fraction and yield in Figs. 2 and 3. Since surface growth dominates the total soot formation, the maximum soot volume fraction monotonically decreases and no synergistic phenomenon can be observed for both preheated and non-preheated cases, following the variation trend of the maximum surface growth rate. Although the variations of the maximum inception and PAH condensation rates show synergistic phenomenon, they cannot modify the variation trend of the maximum soot volume fraction, because of the much lower absolute values than the surface growth rate and the positions where the maximum inception and PAH condensation occur being different from that where the maximum total surface growth occurs.

Soot yield is the integrated mass flow rate of soot at each section above the burner exit. Inception and PAH condensation sub-processes modify the total soot formation rates, although their maximum rates occurs in the centreline region of a flame while the maximum total rate, depending on  $C_2H_2$  addition rate, occurs in the flame wing region. As a result, the variation trend of the maximum soot yield deviates from those of  $C_2H_2$  addition and total surface growth rates. However, because the rates of inception and PAH condensation are much smaller than that of  $C_2H_2$  addition, the variation trend of the maximum soot

yield does not completely follow those of the maximum inception and PAH condensation rates. Consequently, a synergistic phenomenon for the variation of the maximum soot yield is observed in Fig. 3 for the preheated case. The synergistic phenomenon cannot be observed for the non-preheated case because the synergistic phenomenon in the variations of the inception and PAH condensation rate is not strong enough. Therefore, essentially the synergistic phenomenon for soot formation in the preheated ethylene/methane mixture is caused by the inception and PAH condensation processes.

The monotonic decrease in the maximum  $C_2H_2$  addition rate is caused by the decrease in the concentration of  $C_2H_2$  when the fraction of carbon from methane increases, as shown in Fig. 6. The decrease of the maximum  $C_2H_2$  concentration and  $C_2H_2$  addition rate in the non-preheated case is faster than in the preheated case, since flame temperature increases in the preheated case but decreases in the non-preheated case, as shown in Fig. 7. The temperature decrease in the non-preheated case is due to the lower adiabatic temperature of methane flame than that of ethylene flame. In the preheated case, the temperature increase is due to the reduction in radiation heat loss owing to the variation in soot volume fraction, although the temperatures of fuel mixture and air have been adjusted to keep a constant adiabatic temperature.

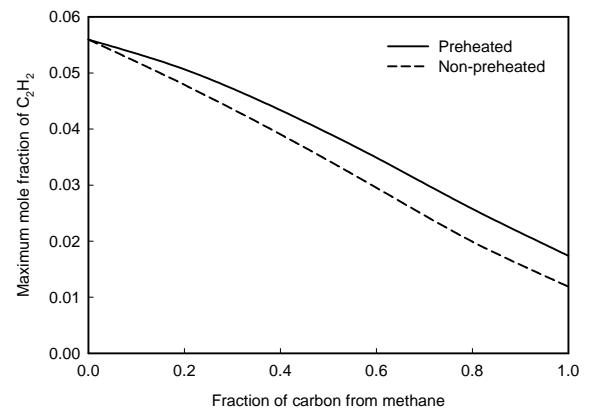


Fig. 6 Variation of maximum  $C_2H_2$  mole fraction.

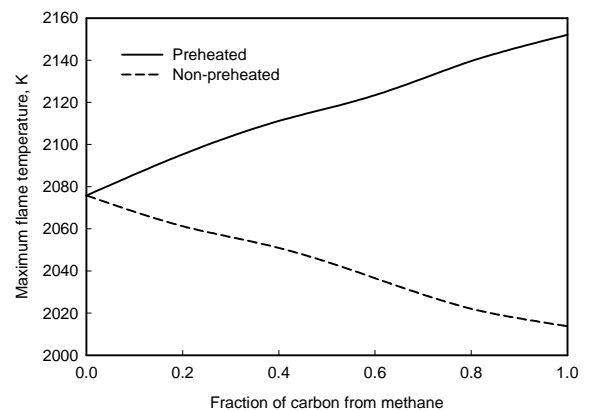


Fig. 7 Variation of maximum flame temperature.

In the numerical model, the inception is assumed to be due to the coagulation of two PAH species, and the PAH condensation is due to the PAH species sticking to particle surface. In this paper, the PAH for inception and condensation is pyrene (A4). Therefore, we can figure out the reason for the synergistic phenomenon by examining the variation in the concentration of pyrene. The variation of the maximum pyrene mole fraction is displayed in Fig. 8, which shows a similar variation trend as those for inception and PAH condensation rates. In the gas phase chemistry employed in this paper and originally developed by Appel et al. [10], the formation of pyrene is closely related to that of benzene (A1). A pathway analysis suggests that the primary formation reaction of benzene is the recombination of propargyl radicals  $C_3H_3 + C_3H_3 \Rightarrow A1$ . The variation of the maximum concentration of  $C_3H_3$  is also shown in Fig. 8. We note that the variation trend of propargyl radical shows the synergistic phenomenon over the range of ethylene/methane mixture. Therefore, the synergistic phenomenon can be examined by further tracking the formation of  $C_3H_3$ .

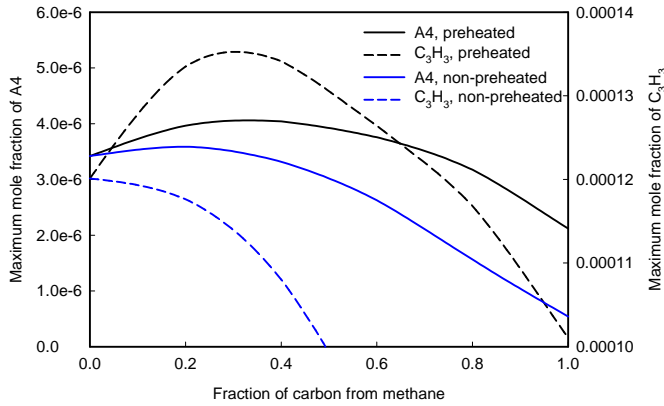


Fig. 8 Variations of pyrene (A4) and propargyl ( $C_3H_3$ ).

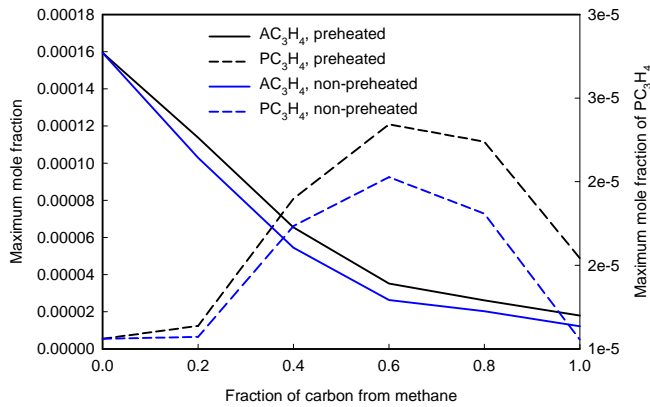


Fig. 9 Variations of  $AC_3H_4$  and  $PC_3H_4$ .

The pathway analysis indicates that the two important formation reactions of  $C_3H_3$  are  $AC_3H_4 + H = C_3H_3 + H_2$  and  $PC_3H_4 + H = C_3H_3 + H_2$ . Since the flame temperatures do not change very much, as shown in Fig.7, the formation of  $C_3H_3$  mainly depends on the concentrations of H,  $AC_3H_4$  and  $PC_3H_4$ . The simulation shows and it is easy to understand that the

concentration of H radical monotonically increases with the increase in the fraction of carbon from methane. Therefore, we only examine the variations of  $AC_3H_4$  and  $PC_3H_4$  concentrations. Figure 9 shows that  $AC_3H_4$  monotonically decreases, whereas  $PC_3H_4$  first increases and then decreases, when the fraction of carbon from methane increases. Accordingly, the synergistic phenomenon is caused by the variation in the formation of  $PC_3H_4$ .

Further analysis reveals that the primary formation reaction of  $PC_3H_4$  is  $C_2H_2 + CH_3 = PC_3H_4 + H$ , suggesting that the formation of  $PC_3H_4$  depends on the concentrations of  $C_2H_2$  and  $CH_3$ . Figure 10 shows that the concentration of  $CH_3$  monotonically increases with the increase in the fraction of carbon from methane. This is easy to understand, since methane produces more  $CH_3$ . The concentration of  $C_2H_2$  monotonically decreases, as shown in Fig. 6. Therefore, the combined effects of the variations in the concentrations of  $C_2H_2$  and  $CH_3$  result in the synergistic phenomenon in the variation of  $PC_3H_4$  and finally the variation of the maximum soot yield for the preheated case in Fig. 3. For the non-preheated case, the slighter synergistic phenomenon in the variation of  $PC_3H_4$  cannot cause the final synergistic phenomenon in the maximum soot yield.

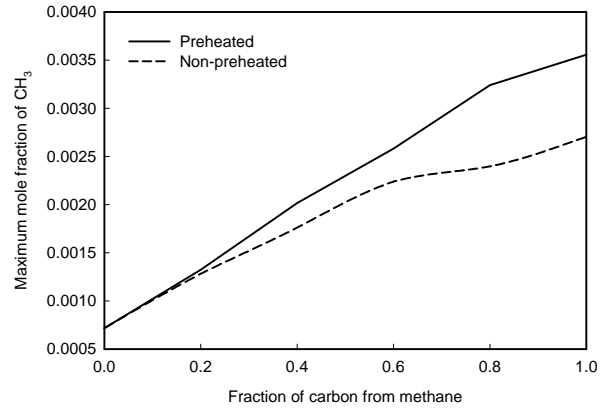


Fig. 10 Variation of  $CH_3$ .

## CONCLUSIONS

The characteristics of soot formation in laminar diffusion flames employing ethylene/methane mixture have been investigated by detailed numerical simulation. The numerical results have qualitatively captured the phenomena observed experimentally. A synergistic phenomenon is observed for the variation of the maximum soot yield over the range of ethylene/methane mixture when the temperatures of both fuel mixture and air are preheated so that the adiabatic flame temperature are same for all the flames. Detailed analysis of the numerical results suggests that the synergistic phenomenon is caused by the combined effects of the variations in the concentrations of  $C_2H_2$  and  $CH_3$  radical. When the fraction of carbon from methane in fuel mixture increases, the concentration of  $C_2H_2$  monotonically decreases, whereas that of  $CH_3$  radical increases, resulting in the synergistic phenomenon in the variation of  $C_3H_3$  radical concentration, due to the

reactions  $C_2H_2 + CH_3 = PC_3H_4 + H$  and  $PC_3H_4 + H = C_3H_3 + H_2$ . This synergistic phenomenon causes a qualitatively similar variation trend in the concentration of pyrene. Consequently, the synergistic effect occurs for soot inception and PAH condensation rates, leading to the synergistic phenomenon in soot yield. The similar synergistic phenomenon is not observed in the variation of peak soot volume fraction, since the maximum surface growth rate monotonically decreases, as the fraction of carbon from methane in fuel mixture increases. As for the non-preheated case, the slighter synergistic phenomenon in the variation of  $PC_3H_4$  is not enough to cause the final synergistic phenomenon in the maximum soot yield.

## REFERENCES:

1. Frenklach, M., Yuan, T., Ramachandra, M.K., 1988, "Soot formation in binary Hydrocarbon mixtures", *Energy Fuels* 2 (1998) 462-480.
2. Hwang, J.Y., Chung, S.H., Lee, W., Kang, G., Chun, S.H., 1998, "Synergistic effect of ethylene-propane mixture on soot formation in laminar diffusion flames", *Combust. Flame*, 114, pp.370-380.
3. Hwang, J.Y., Chung, S.H., Lee, W., 1998, "Effects of oxygen and propan addition on soot formation in counterflow ethylene flames and the role of  $C_3$  chemistry", *Prod. Combust. Inst.*, 27, pp.1531-1538.
4. Frenklach, M., 1988, "On the driving force of PAH production", *Prod. Comb. Inst.*, 21, pp.1075-1082.
5. Miller, J.A., Melius, C.F., 1992, "Kinetic of thermodynamic issues in the formation of aromatic compounds in flames of aliphatic fuels", *Combust. Flame*, 91, pp.21-39.
6. Roesler, J.R., Martinot, S., McEnally, C.S., Pfefferle, L.D., Delfau, J.-L., Vovelle, C., 2003, "Investigating the role of methane on the growth of aromatic hydrocarbons and soot in fundamental combustion processes", *Combust. Flame*, 134, pp.249-260.
7. Trottier, S., Guo, H., Smallwood, G.J., Johnson, M.R., 2007, "Measurement and modeling of the sooting propensity of binary fuel mixtures", *Prod. Combust. Inst.*, 31, pp.611-619.
8. McEnally, C.S., Pfefferle, L.D., 2007, "The effect of dimethyl ether and ethanol on benzene and soot formation in ethylene nonpremixed flames", *Proc. Combust. Inst.*, 31, pp.603-610.
9. Frenklach, M., H. Wang, H., 1994, in: Bockhorn, H., (Eds), *Soot Formation in Combustion: Mechanisms and Models*, Vol. 59, Springer-Verlag, Berlin, pp. 162 - 196.
10. Appel, J., Bockhorn, H., and Frenklach, M., 2000, "Kinetic modeling of soot formation with detailed chemistry and physics: laminar premixed flames of  $C_2$  hydrocarbons", *Combust. Flame*, 121, pp.122-136.
11. Guo, H., Liu, F., Smallwood, G.J., and Gülder, Ö.L., 2002, "The flame preheating effect on numerical modelling of soot formation in a two-dimensional laminar ethylene-air diffusion flame", *Combust. Theory Modelling*, 6, pp.173-187.
12. Patankar, S.V., 1980, *Numerical Heat Transfer and Fluid Flow*, Hemisphere, New York.
13. Liu, Z., Liao, C., Liu, C. and McCormick, S., 1995, "Multigrid method for multi-step finite rate combustion", 33<sup>rd</sup> Aerospace Science Meeting and Exhibit (AIAA paper 95-0205), January 9-12, Reno, NV.
14. Kee, R.J., Miller, J.A., and Jefferson, T.H., 1980, "A General-Purpose, Problem-Independent, Transportable, Fortran Chemical Kinetics Code Package", Sandia Report, SAND 80-8003, Sandia National Laboratories.
15. Kee, R.J., Dixon-Lewis, G., Warnatz, J., Coltrin, M.E., and Miller, J.A., 1986, "A Fortran computer code package for the evaluation of gas-phase, multicomponent transport properties", Report No. SAND 86-8246, Sandia National Laboratories.
16. Liu, F., Guo, H., Smallwood, G.J., Gülder, Ö.L., 2004, "Effect of radiation model on the modeling of a laminar coflow methane/air diffusion flame", *Combust. Flame*, 138, pp.136-154.